Geoderma 463 (2025) 117602

Contents lists available at ScienceDirect

Geoderma

journal homepage: www.elsevier.com/locate/geoderma

Organic fertilization under conservation tillage enhances biopore formation and particulate organic matter accumulation via fraction-specific pore relationships in a Vertisol

Tianyu Ding [a,c], Zichun Guo [a,*], John Koestel [b], Jiaqi Li [a,d], Jianli Liu [a,c], Xinhua Peng [e]

[a] State Key Laboratory of Soil and Sustainable Agriculture, Institute of Soil Science, Chinese Academy of Sciences, Nanjing 211135, PR China
[b] Department of Soil and Environment, Swedish University of Agricultural Sciences, Box 7014, 750 07 Uppsala, Sweden
[c] University of the Chinese Academy of Sciences, Nanjing 211135, PR China
[d] College of Land Resources and Environment, Jiangxi Agriculture University, Nanchang 330045, PR China
[e] State Key Laboratory of Efficient Utilization of Arable Land in China, Institute of Agricultural Resources and Regional Planning, Chinese Academy of Agricultural Sciences, Beijing 100081, PR China

ARTICLE INFO

Handling Editor: Yvan Capowiez

Keywords:
Soil macropore structure
Biopore
Particulate organic matter (POM)
Organic fertilization
X-ray CT
Vertisol
Conservation tillage

ABSTRACT

Understanding how fresh, decomposed, and root-derived particulate organic matter (POM) interact with soil macropores is crucial for enhancing soil organic carbon stocks, yet their spatial relationships remain largely unclear. Therefore, we conducted an 8-year conservation tillage experiment on a Vertisol (wheat-maize rotation, no tillage with straw return) that compared four fertilization regimes: (i) control (no fertilization), (ii) chemical fertilization (NPK), (iii) organic fertilization (OF), and (iv) combined chemical-organic fertilization (NPKOF). X-ray computed tomography was used to quantify POM fractions, macropore and biopore structure. Our results demonstrated that all fertilization treatments (NPK, OF, NPKOF) significantly improved soil macropore structure in the 0–10 cm layer, whereas OF and NPKOF increased bioporosity by 4.82-fold and 2.26-fold in the 10–20 cm layer ($P < 0.05$). Biopores constitute a major component of percolating pores in the subsoil and are promoted by the application of organic fertilization. Furthermore, OF and NPKOF significantly enhanced fresh POM and root-derived POM content in the 0–10 cm layer and shortened their distance to pores throughout the 0–20 cm layer ($P < 0.05$). The three POM fractions exhibited positive correlations with macropore structure characteristics ($P < 0.05$), yet no significant correlation was observed between root-derived POM and biopores. Root-derived POM showed preferential accumulation in areas distant from biopores. Overall, our findings demonstrate that long-term organic fertilization is linked to increased POM accumulation, improvements in surface soil macropore structure, and enhanced biopore formation in the subsoil of Vertisols.

1. Introduction

Soil macropore structure refers to the three-dimensional arrangement of voids formed by the solid components of soil across different scales. Macropore structure is critically linked to soil functions, as it provides habitats for numerous soil organisms and mediates key biochemical reactions (Rabot et al., 2018). In agricultural soils, optimizing pore structure enhances root growth, improves nutrient availability, and increases crop productivity (Zhang and Peng, 2021; Liu et al., 2025). Based on formation mechanisms and morphological characteristics, soil macropores can be classified into two major categories: biopores and nonbiopores. Biopores are directly formed by soil biological activity, including root penetration, decay-induced channels, and burrowing by earthworms and other soil fauna (Lucas et al., 2019; Kautz, 2014; Behringer et al., 2025; Capowiez et al., 2021). They play a vital role in regulating water movement and sustaining pore network development (Phalempin et al., 2025a; Zhang et al., 2019), thereby directly influencing soil organic matter (SOM) dynamics and nutrient cycling.

As a labile component of SOM, particulate organic matter (POM) originates primarily from plant residues. It is characterized by its large particle size, high carbon-to-nitrogen ratio, low density, and high microbial degradability (Lavallee et al., 2020). Traditional POM quantification methods rely on particle size and density fractionation, which

* Corresponding author.
E-mail address: zcguo@issas.ac.cn (Z. Guo).

https://doi.org/10.1016/j.geoderma.2025.117602
Received 5 September 2025; Received in revised form 6 November 2025; Accepted 9 November 2025
Available online 11 November 2025

disrupts soil structure. In contrast, X-ray computed tomography (CT) combined with machine learning enables in situ POM quantification while preserving spatial distribution information. Based on its origin and morphological features, POM can be classified into three distinct fractions: (1) fresh POM, (2) decomposed POM, and (3) root-derived POM (Schlüter et al., 2022b; Phalempin et al., 2025a; Leuther et al., 2022). Fresh POM consists of coarse, undecomposed residues (e.g., straw and leaves) and is typically found in macropores. Decomposed POM primarily comprises biochar or fragmented residues from further decomposition of fresh POM. Root-derived POM is associated with root growth and penetration, often contributing to biopore formation (Lucas et al., 2023). Therefore, quantifying POM into these three fractions is crucial for elucidating its accumulation mechanisms in soils.

Macropore structure directly governs water and gas transport, thereby influencing microbial decomposition of POM (Kravchenko and Guber, 2017). Previous studies have demonstrated that macropore size and connectivity can enhance POM decomposition (Kravchenko et al., 2015; Ding et al., 2025b). Schlüter et al. (2022b) observed that POM decomposition resulted in organic carbon enrichment within a 30–60 μm radius around decomposing POM. However, existing studies have primarily focused on the relationship between POM and macropore structures, while the role of biopores in regulating POM loss or accumulation, particularly root-derived POM, remains poorly understood. During root penetration, the redistribution of soil particles may either expose fresh POM and decomposed POM to pore spaces or encapsulate them within the soil matrix (Leuther et al., 2023). Notably, large, continuous biopores exhibited complete connectivity, forming the backbone of complex pore networks (Koestel et al., 2018b). Furthermore, biopores play a crucial role in regulating subsurface water movement and gas exchange, processes that directly control POM dynamics (Zhang et al., 2019; Lee et al., 2024a). Establishing quantitative relationships between biopores and POM fractions (fresh POM, decomposed POM, and root-derived POM) is therefore essential for understanding biologically mediated POM dynamics in soils.

Shajiang black soil, covering an area of 4×10^6 ha in North China Plain, is a typical soil type producing low-to-medium crop productivity in China. It is characterized by high clay content, high soil strength, increased bulk density, and low organic matter content (Peng et al., 2022). To enhance crop productivity, local farmers commonly apply chemical fertilizers to provide essential nutrients. While chemical fertilizers can promote POM accumulation by increasing root biomass and crop residue returns (Ding et al., 2025a), they may also introduce dispersive ions, such as NH_4^+ and Na^+, that promote soil compaction and structural degradation (Guo et al., 2022; Guo et al., 2019). Several studies have demonstrated that chemical fertilizers failed to improve soil macropore structure relative to no fertilization (Yu et al., 2025; Fang et al., 2024). In contrast, organic fertilizers not only enhance POM accumulation through organic matter inputs but also significantly improve soil structure (Zhou et al., 2016; Leuther et al., 2022). Conservation tillage (no-tillage with straw mulching) is recognized as a key agricultural practice for improving soil structure and maintaining soil productivity (Ren et al., 2024; Jiang et al., 2024). The integration of organic fertilization with conservation tillage may provide a viable strategy for enhancing Vertisol structure and increasing organic matter accumulation. Despite these benefits, the mechanisms governing POM dynamics (fresh, decomposed, and root-derived POM) in relation to pore structure, especially biopores, under organic fertilization under conservation tillage remain unclear. In this study, we hypothesized that long-term organic fertilization could increase POM content and improve biopore structure, and root-derived POM content was strongly associated with biopore abundance. To test these hypotheses, we analyzed soil samples from an 8-year field experiment comparing four fertilization regimes under conservation tillage in Vertisols: (i) control (no fertilization), (ii) chemical fertilization, (iii) organic fertilization, and (iv) combined chemical-organic fertilization. Our specific objectives were to: (i) quantify the effects of different fertilization regimes on POM distribution and pore structure (macropores and biopores), and (ii) establish quantitative relationships between POM fractions and pore characteristics.

2. Materials and methods

2.1. Experimental site

The field experiment was established in October 2015 in Longkang Farm (33°32′ N, 115°59′ E), Anhui Province, China. The mean annual temperature and precipitation were 14.8 °C and 912 mm. The soil is derived from fluvial-lacustrine sediments, classified as a Vertisol according to the USDA Soil Taxonomy. It exhibited a clay loam texture (8 % sand, 54.1 % silt, and 37.9 % clay), with an initial soil organic carbon (SOC) content of 8.84 g kg^{-1} in the 0–20 cm layer.

The experiment was conducted in a maize-wheat rotation system under conservation tillage management. The experimental field was maintained under a no-tillage regime for the entire year. After crop harvest, the straw was chopped into segments (<15 cm) and returned to the field as mulch, followed by fertilizer application. Four fertilization treatments were applied in a randomized complete block design: no fertilization (control), chemical fertilization (NPK), organic fertilization (OF), and combined chemical and organic fertilization (NPKOF). Each plot measured 160 m^2 (20 m × 8 m), with three replications per treatment. In the NPK treatment, fertilizers were applied at 210 kg N ha^{-1}, 60 kg P_2O_5 ha^{-1}, and 90 kg K_2O ha^{-1} for each season. A basal application of 100 kg N ha^{-1} along with all P and K fertilizers was applied before sowing, with the remaining 110 kg N ha^{-1} applied during stem elongation. For the OF treatment, commercial organic fertilizer (8194 kg ha^{-1}; containing > 4 % N + P_2O_5 + K_2O and > 30 % soil organic matter) was applied before sowing each season. In the NPKOF treatment, a combination of commercial organic fertilizer (4097 kg ha^{-1}), 50 kg N ha^{-1}, 11.3 kg P_2O_5 ha^{-1}, and 33.4 kg K_2O ha^{-1} was applied before sowing, followed by an additional 55.1 kg N ha^{-1} during stem elongation each season.

2.2. Soil sampling and measurements

Undisturbed soil samples were collected using PVC cores (5 cm diameter, 5 cm height) in September 2024 from the 0–10 cm and 10–20 cm layers. A total of 24 PVC cores were sampled (3 replicates × 2 soil layers × 4 treatments). Each PVC core was sealed with plastic film and stored at 4 °C until CT scanning. Additionally, steel ring knife samples were collected from both soil layers to determine soil physical properties, including air permeability (K_a), saturated hydraulic conductivity (K_s), and bulk density. Furthermore, composite soil samples (4–5 random sampling points per plot) were collected and homogenized for soil organic carbon (SOC) analysis (Lu, 2000).

The small cores were initially saturated in a sandbox with the bottom 3 cm immersed in water, followed by drainage to −100 hpa water potential. K_a was measured using the steady-state method and calculated according to Darcy's law (Yi, 2009; Zhang et al., 2019):

$$K_a = \frac{QL\eta}{A\Delta P} \quad (1)$$

where Q is the air flow rate (L^3 T^{-1}), L is the sample length (L), η is the dynamic air viscosity (M L^{-1} T^{-1}), A is the cross-sectional area (L^2), and ΔP is the pressure difference (M L^{-1} T^{-2}). K_s was measured using the constant head method (Yi, 2009) after resaturating the soil cores. SOC was measured using the potassium dichromate heating method described by Lu (2000).

2.3. X-ray CT scanning and image analysis

2.3.1. X-ray CT scanning

PVC cores were scanned using an industrial X-ray CT scanner (v|

tome|x m 300) in multi-scan mode at settings of 160 kV and 160 μA. Each core was scanned at a voxel size of 30 μm using a detector with a 2024 × 2024 pixel array. The image resolution is approximately 90 μm, which is three times the voxel resolution (Behringer et al., 2025). The reconstructed 3D volumetric data were exported as 16-bit grayscale TIFF format images using VG Studio MAX 3.5 software. Image preprocessing was performed using Fiji software (Schindelin et al., 2012), which included brightness/contrast adjustment and application of a median filter for noise reduction. Then, a cylindrical region of interest (ROI) measuring 40.5 mm in diameter and 39 mm in height was extracted from each core for further analysis (Fig. 1a).

2.3.2. POM determination

Image analysis was performed using Fiji and Ilastik software. Soils were segmented into pores, POM, and matrix via Ilastik pixel classification (Fig. 1a), an interactive machine-learning tool (Berg et al., 2019). A random forest classifier was trained on the gray images, utilizing a multi-dimensional feature space that included gray values and intensity gradients. POM was further classified into fresh POM, decomposed POM and root-derived POM based on morphological characteristics including blobness, compactness, plateness, and sphericity (Table S1) (Schlüter et al., 2022b; Leuther et al., 2022). These morphological parameters were obtained using the "Connected Components Labeling" and "Analyze Regions 3D" tools within the MorphoLibJ plugin (Legland et al., 2016). Decomposed POM exhibited the most compact morphology, characterized by the highest values of compactness, plateness, and sphericity among all POM fractions. In contrast, root-derived POM displayed elongated cylindrical shapes with minimal blobness. Fresh POM showed intermediate morphological characteristics across all measured parameters. Firstly, POM was classified into fresh residues (including roots and fresh POM) and decomposed POM. A training dataset consisting of 1,322 manually labeled POM was classified into fresh residues and decomposed POM (Fig. 1b). The dataset was randomly divided into training (n = 925) and validation subsets (n = 397). We implemented a random forest classifier with 500 decision trees in Python 3.12, which achieved 94.5 % prediction accuracy on the

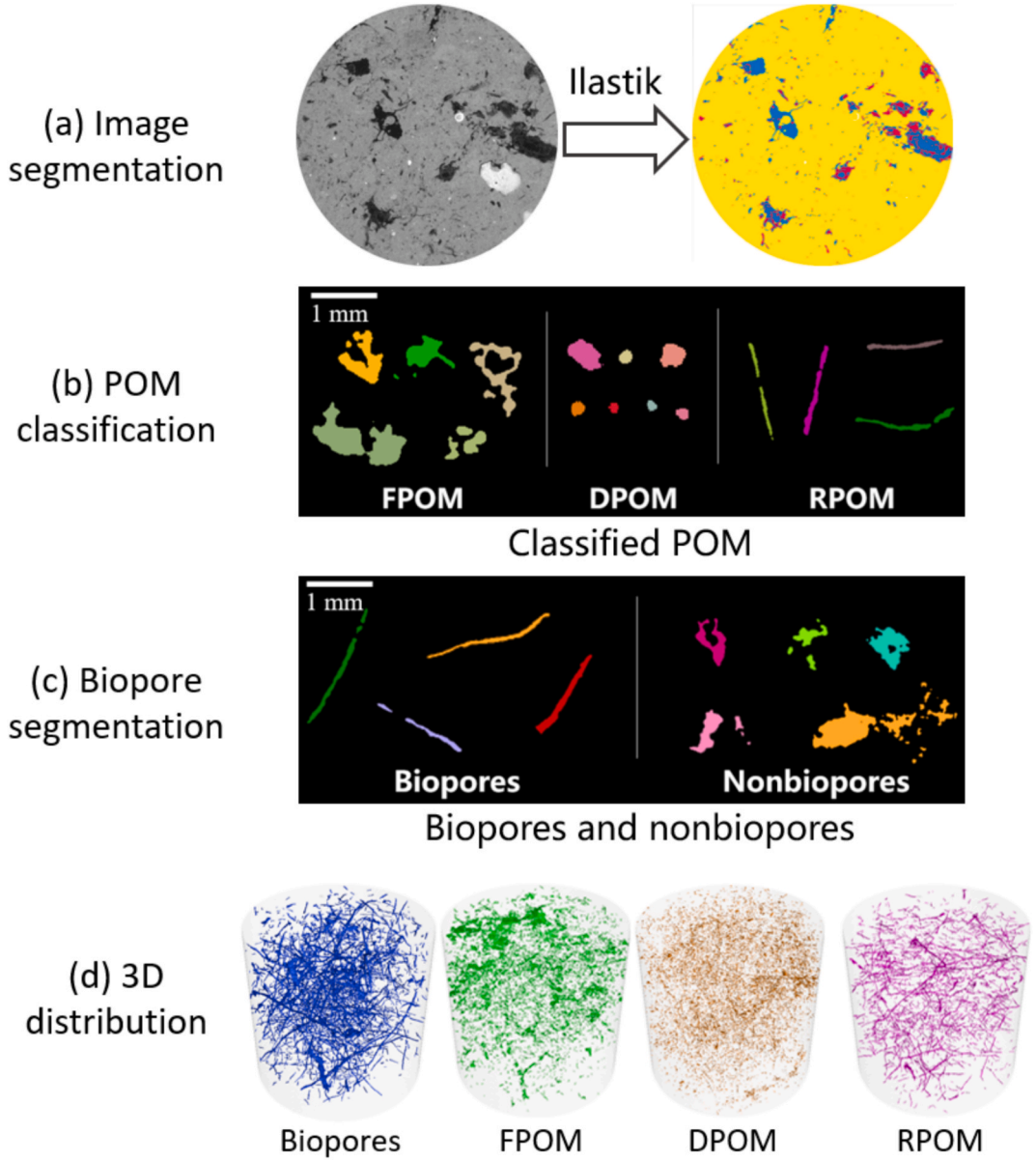

Fig. 1. Image processing flowchart. FPOM, DPOM and RPOM indicate fresh POM, decomposed POM, and root-derived POM. The yellow, red, and blue parts represent soil matrix, POM and macropores in Fig. a. The green, brown, pink, and blue parts represent fresh POM, decomposed POM, root-derived POM, and biopores, respectively in Fig. d.

validation subset. Subsequently, the classifier was retrained using the complete training dataset, yielding an out-of-bag (OOB) error rate of 6.6 % (Table S2). The optimized classifier was then applied to classify the entire sample set. Finally, classification results were assigned to labeled POM images using the "Assign measure to label" function in MorphoLibJ. Subsequently, fresh residues were classified into root-derived POM and fresh POM. An additional 967 manually selected observations comprising both fresh POM and root-derived POM were used to train a secondary random forest classifier (Fig. 1b). This model achieved a prediction accuracy of 93.1 % with an OOB error rate of 7.8 % for distinguishing between fresh and root-derived POM (Table S3). Notably, some root-derived POM fragments remained connected to fresh POM in the segmented images. These connections were resolved using "Distance Transform Watershed 3D", followed by manual reclassification of non-root POM fragments as fresh POM. POM content was calculated using the "Analyze Region 3D" tool and POM length density was obtained by "Skeletonise" and "Analyze Skeleton" in Fiji. Previous studies have typically classified roots within the fresh POM fraction (Schlüter et al., 2022b). In our study, we specifically isolated roots as a distinct category to enable precise analysis of biopore-POM relationships.

2.3.3. Macropore determination and biopore segmentation

The image-based porosity was calculated as the percentage of CT-derived pore voxels relative to the total voxels in the ROI. The connected porosity, defined as the volume fraction of interconnected pores, was quantified using the "Purify" in Fiji. Mean pore diameter and pore size distributions were quantified using the "Local thickness" package, based on the maximum inscribed sphere method. Macropore sizes were divided into 4 classes: 60–150 μm, 150–300 μm, 300–500 μm, and > 500 μm. The hydraulic radius was calculated by the ratio of pore volume to macropore surface area (Larsbo et al., 2014). The surface area density was determined using the "Analyze Region 3D" tool. Connection probability, a metric used to evaluate macropore network connectivity, ranges from 0 (many unconnected pores) to 1 (all pores forming a single interconnected cluster). It was calculated using the formula described by Renard and Allard (2013):

$$\Gamma = \sum_{i=0}^{n} V_i^2 / \left(\sum_{i=0}^{n} V_i \right)^2 \tag{2}$$

where Γ is the connection probability, V_i the volume of each macropore, and n the total number of macropores. The volume and surface area of each macropore were measured using the "Connected Components Labeling" and "Analyze region 3D" tools in the MorphoLibJ plugin. The average POM-macropore distance was derived as a frequency-weighted mean of the Euclidean distances between individual POM voxels and their nearest pores (Schlüter and Vogel, 2016). This metric serves as an indicator of POM occlusion within the soil matrix. The critical macropore diameter was obtained using the SoilJ plugin (Koestel, 2018a). Due to the limited resolution, percolating pores connecting the top to the bottom of the ROI could not be detected in several cores. Consequently, a critical macropore diameter could not be determined for these samples.

The biopore segmentation followed the same methodology as root-derived POM segmentation. We established a training dataset comprising 807 manually classified observations (biopores and non-biopores) (Fig. 1c). Using this dataset, a random forest classifier achieved 96.3 % prediction accuracy with a 4.09 % out-of-bag (OOB) error rate (Table S4), which was subsequently applied to classify all pores in the samples. Notably, many non-biopores connected to biopores were initially misclassified. To address this, we implemented an image processing pipeline beginning with single-pixel erosion of biopore boundaries, followed by Distance Transform Watershed 3D to achieve complete separation. The refined pore network was then reclassified using the random forest classifier, with subsequent single-pixel dilation of biopores to restore original dimensions. Final manual correction was required to address two specific artifacts: few non-biopore misclassifications and the loss of fine biopore structures (1–2 pixels wide) resulting from the erosion process, thereby ensuring segmentation accuracy. This was conducted using "Connected Components Labeling" and "Label Edition" in Fiji. The characteristic parameters of biopores were calculated using the same methodology applied for pores and root-derived POM. Visualization of the 3D biopore structure and POM was achieved with VG Studio MAX 2022 software (Fig. 1d).

2.4. Estimate of carbon (C) input from crops

The C input (Mg ha^{-1} yr^{-1}) from crops was estimated as the sum of C derived from roots and stubble ($C_{root+stubble}$) and straw (C_{straw}), calculated using the following equations (Hua et al., 2014; Zhao et al., 2018; IPCC, 2006; NCATS, 1999):

$$C_{input} = C_{straw} + C_{root+stubble} \tag{3}$$

$$C_{straw} = (Y_{grain} \times \lambda \times OC_{crop}) \times (1 - W) \div 1000 \tag{4}$$

where Y_{grain} is the grain yield; λ is the ratio of straw to grain (1.2 for maize, 1.1 for wheat); OC_{crop} is the C content of air-dried crop (444 g kg^{-1} for maize, 399 g kg^{-1} for wheat); W is the average water content of air-dried gain (0.14 g g^{-1}).

$$C_{root+stubble} = ((Y_{grain} + Y_{straw}) \times R \times R_{root} + R_{stubble} \times Y_{straw}) \times (1 - W) \times OC_{crop} \div 1000 \tag{5}$$

where Y_{straw} is the straw yield (kg ha^{-1}); R is the ratio of root biomass to total aboveground biomass (0.351 for maize, 0.429 for wheat); R_{root} is the ratio of the root system within the topsoil (0–20 cm) (0.851 for maize, 0.753 for wheat); $R_{stubble}$ is the coefficient of stubble (0.03 for maize, 0.13 for wheat).

2.5. Statistical analysis

Data analysis was conducted using SPSS 23.0 and Origin 2017. One-way analysis of variance (ANOVA) was used to assess the impact of different fertilizations on POM, macropore and biopore structure parameters. Post-hoc comparisons were performed using the least significant difference (LSD) method at a 5 % significance level. When the assumptions of ANOVA were not fulfilled, the Kruskal-Walli's test was employed to assess the statistical significance of differences. The Cohen's d effect size was calculated to quantify the differences between treatment and control groups (Table S5-S12). Spearman correlation analysis was applied to examine the relationship between POM and macropore, biopore structure. Furthermore, partial correlation analysis was performed to evaluate the relationship between POM and pore characteristics while controlling for the effects of K_a, K_s, SOC, and bulk density.

3. Results

3.1. Soil basic properties

Compared to the control treatment, the NPK, OF, and NPKOF treatments exhibited a significant increase in K_a and K_s in the 0–10 cm layer ($P < 0.05$, Table 1). The OF and NPKOF treatments significantly increased the SOC by 207 % and 120 %, respectively, in the 0–10 cm layer, and 38.9 % and 44.4 % in the 10–20 cm layer ($P < 0.05$). Furthermore, the NPK, OF, and NPKOF treatments also decreased bulk density by 6.3 %, 13.8 %, and 14.4 %, respectively, in the 0–10 cm layer ($P < 0.05$).

Table 1
Soil basic properties under different fertilization regimes. NPK, OF and NPKOF indicate treatments of chemical fertilizations, organic fertilization, and combined chemical fertilization with organic fertilization, respectively. Different lowercase letters indicate significant differences among various fertilization regimes ($P < 0.05$).

	Treatments	Bulk density /g cm^{-3}	LnK_s /10^{-5} mm h^{-1}	LnK_a /10^{-3} μm^2	SOC /g kg^{-1}
0–10 cm	Control	1.60 (0.00) a	12.3 (0.95) b	4.71 (0.43) b	12.3 (1.04) c
	NPK	1.50 (0.06) b	13.6 (2.86) a	8.29 (0.45) a	14.3 (0.18) c
	OF	1.38 (0.02) c	15.0 (1.65) a	8.68 (1.26) a	37.8 (2.33) a
	NPKOF	1.37 (0.08) c	13.4 (3.34) a	8.44 (1.43) a	27.0 (1.11) b
10–20 cm	Control	1.66 (0.05) a	11.0 (2.93) a	5.17 (1.06) a	6.64 (0.69) c
	NPK	1.65 (0.05) a	11.7 (1.14) a	5.83 (0.40) a	7.95 (0.13) bc
	OF	1.62 (0.02) a	13.7 (2.41) a	5.90 (0.22) a	9.22 (1.01) ab
	NPKOF	1.62 (0.07) a	11.3 (2.31) a	4.87 (1.57) a	9.59 (0.82) a

3.2. Macropore structures

The image-based porosity in the 0–10 cm layer was significantly greater in the NPK, OF, and NPKOF treatments than in the control, with values higher by 233 %, 283 %, and 224 %, respectively ($P < 0.05$; Fig. 2a). Significant differences between these fertilized treatments and the control were also observed for porosity across four size classes (60–150 μm, 150–300 μm, 300–500 μm, and > 500 μm), as well as for connected porosity and connection probability in the 0–10 cm layer ($P < 0.05$, Fig. 2, Table 2). Notably, the mean pore diameter and surface area density in the 0–10 cm layer were 42.3 % and 128 % greater, respectively, under the OF treatment compared to the control ($P < 0.05$). In the 10–20 cm layer, the OF treatment exhibited significantly higher values for total image-based porosity, porosity in the 150–300 μm, 300–500 μm, and > 500 μm size classes, connected porosity, and connection probability relative to the control ($P < 0.05$). The NPKOF treatment also showed significantly greater connected porosity and connection probability in the 10–20 cm layer than the control ($P < 0.05$). Furthermore, no critical macropore diameter was detected in the control treatment (Table 2).

3.3. Biopore structures

The representative 3D visualizations of biopore networks under various fertilization treatments are shown in Fig. 3. In the 0–10 cm soil layer, the control treatment primarily exhibited finer biopores, while the NPK and NPKOF treatments showed more interconnected and structurally elaborate biopore networks containing root-derived biopores or burrows. In the 10–20 cm layer, both OF and NPKOF treatments demonstrated more densely clustered and highly branched biopore networks.

Compared to the control treatment, the NPK, OF, and NPKOF treatments exhibited significantly greater bioporosity by 331 %, 111 %, and 358 %, respectively, in the 0–10 cm layer ($P < 0.05$, Fig. 4). In the 0–10 cm layer, the biopore surface area density was significantly higher under both the OF and NPKOF treatments than in the control ($P < 0.05$). In the 10–20 cm layer, these two treatments (OF and NPKOF) also showed significantly greater bioporosity, biopore proportion, mean biopore diameter, and biopore length density compared to the control ($P < 0.05$, Fig. 4, Table 3). Additionally, the NPKOF treatment resulted in a higher biopore length density in the 0–10 cm layer ($P < 0.05$). The hydraulic radius of biopores in the 10–20 cm layer was also significantly larger under the OF treatment ($P < 0.05$).

3.4. POM distributions

The 3D distributions of fresh, decomposed and root-derived POM are presented in Fig. 5. In the 0–10 cm layer, the NPK, OF, and NPKOF treatments exhibited more concentrated and spatially widespread fresh POM distributions compared to the control. At a depth of 10–20 cm, the OF treatment displayed a larger quantity of fresh POM. Regarding root-derived POM, the OF and NPKOF treatments showed a greater distribution in the 0–10 cm layer.

Compared to the control treatment, the NPKOF treatment contained significantly more fresh POM and decomposed POM in the 0–10 cm soil layer, with contents greater by 202 % and 90.4 %, respectively (Fig. 6, $P < 0.05$). The OF treatment also showed significantly higher fresh POM content in both the 0–10 cm and 10–20 cm layers, as well as higher decomposed POM content in the 10–20 cm layer compared to the control ($P < 0.05$). In contrast, the root-derived POM length density was significantly lower in the 0–10 cm layer under the OF treatment and in the 10–20 cm layer under the NPKOF treatment than in the control ($P < 0.05$). Furthermore, when compared to the NPK treatment, the content of root-derived POM in the 0–10 cm layer was 65.7 % and 67.7 % greater under the OF and NPKOF treatments, respectively ($P < 0.05$).

Both OF and NPKOF treatments resulted in a significantly shorter distance from macropores to fresh, decomposed, and root-derived POM in the 0–10 cm layer relative to the control ($P < 0.05$, Fig. 7). A similar reduction in distance to macropores was observed for decomposed and root-derived POM in the 10–20 cm layer under these treatments ($P < 0.05$). Compared to the control, the NPK and NPKOF treatments were associated with a shorter fresh POM-biopore distance and decomposed POM-biopore distance in the 0–10 cm layer ($P < 0.05$). In the 10–20 cm layer, the NPK, OF, and NPKOF treatments all exhibited significantly shorter distances from biopores to all three types of POM than the control ($P < 0.05$). Overall, the fresh POM-macropore distance was shorter than the decomposed POM-pore distance (Fig. S1). The root-derived POM-biopore distance was also significantly shorter than the distances for both fresh and decomposed POM to biopores ($P < 0.05$).

3.5. Yields and estimate of carbon input from crops

The three-year average (2022–2024) yield data are presented in Fig. 8. Relative to the control treatment, wheat yield was 3.43, 1.54, and 2.91 times greater under the NPK, OF, and NPKOF treatments, respectively ($P < 0.05$). Similarly, maize yield was significantly higher in these treatments than in the control, with increases of 83.4 %, 49.7 %, and 92.5 % ($P < 0.05$). Furthermore, the NPK, OF, and NPKOF treatments resulted in a significantly higher C input from both straw and roots ($P < 0.05$).

3.6. Relationships between POM and pores, biopores

The correlation matrix revealed significant relationships between macropore characteristics, biopore metrics, and POM fractions (Fig. 9). Both fresh POM and decomposed POM exhibited significant positive correlations with macropore metrics (image-based porosity, connected porosity, hydraulic radius, connection probability), biopore characteristics (mean biopore diameter, connection probability, length density), and K_a ($P < 0.05$). Root-derived POM was positively correlated with image-based porosity, connected porosity, connection probability, and K_a ($P < 0.05$).

In addition, all three POM fractions were significantly positively correlated with porosity across all size classes ($P < 0.01$, Fig. S2). Specifically, fresh POM showed a significant positive correlation with bioporosity in the 300–500 μm range, whereas decomposed POM correlated positively with bioporosity in both 300–500 μm and > 500 μm size classes ($P < 0.05$). No significant correlation was observed between root-derived POM and biopore size distribution ($P > 0.05$, Fig. S2). Additionally, fresh POM and decomposed POM decreased with

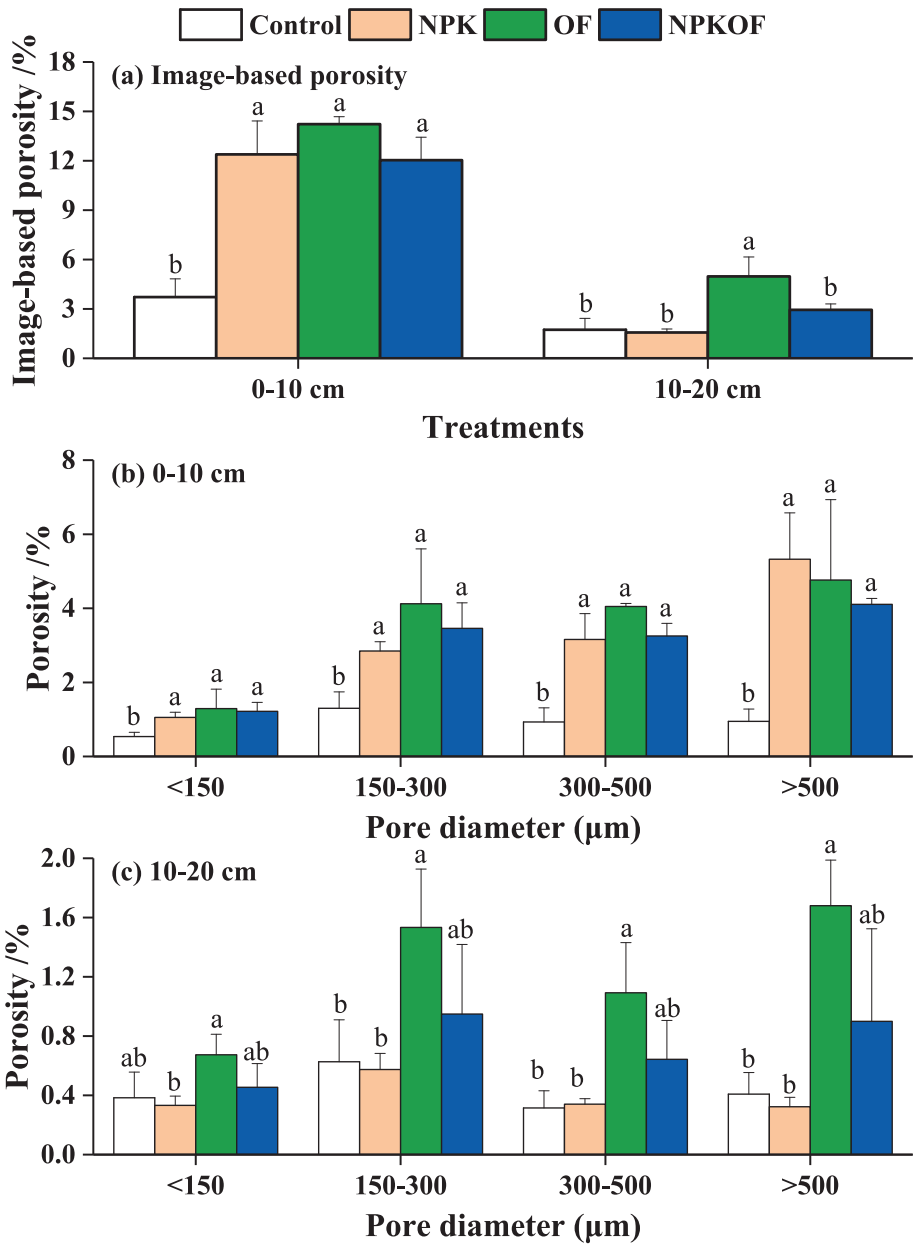

Fig. 2. Image-based porosity and macropore size distributions under different fertilization regimes. NPK, OF and NPKOF indicate treatments of chemical fertilizations, organic fertilization, and combined chemical fertilization with organic fertilization, respectively. Different lowercase letters indicate significant differences among various fertilization regimes ($P < 0.05$).

Table 2
Macropore characteristic parameters under different fertilization regimes. NPK, OF and NPKOF indicate treatments of chemical fertilizations, organic fertilization, and combined chemical fertilization with organic fertilization, respectively. Different lowercase letters indicate significant differences among various fertilization regimes ($P < 0.05$). NA represents there was no percolating macropores due to the limited image resolution.

Pore	Treatments	Connected porosity /%	Mean pore diameter /μm	Critical macropore diameter /μm	Hydraulic radius /μm	Surface area density /mm^{-1}	Connection probability
0–10 cm	Control	2.09 (1.32) b	461 (68.2) b	NA	74.5 (7.39) b	0.50 (0.14) b	0.30 (0.27) b
	NPK	11.9 (2.37) a	636 (26.0) a	325 (n = 3)	109 (11.7) a	0.28 (0.12) c	0.90 (0.04) a
	OF	13.5 (0.50) a	656 (138) a	251 (n = 2)	102 (23.4) ab	1.14 (0.09) a	0.89 (0.04) a
	NPKOF	11.4 (1.42) a	539 (10.1) ab	277 (n = 3)	95.3 (4.44) ab	0.25 (0.04) c	0.88 (0.02) a
10–20 cm	Control	0.44 (0.10) c	434 (11.9) a	NA	63.6 (6.45) a	1.45 (0.36) a	0.10 (0.07) c
	NPK	0.98 (0.27) bc	408 (99.3) a	91.5 (n = 2)	61.7 (1.71) a	0.60 (0.14) b	0.28 (0.09) b
	OF	4.16 (1.31) a	678 (26.8) a	225 (n = 3)	82.2 (0.63) a	1.27 (0.20) a	0.67 (0.12) a
	NPKOF	2.21 (0.38) b	568 (315) a	160 (n = 3)	81.5 (24.5) a	0.39 (0.13) b	0.55 (0.06) a

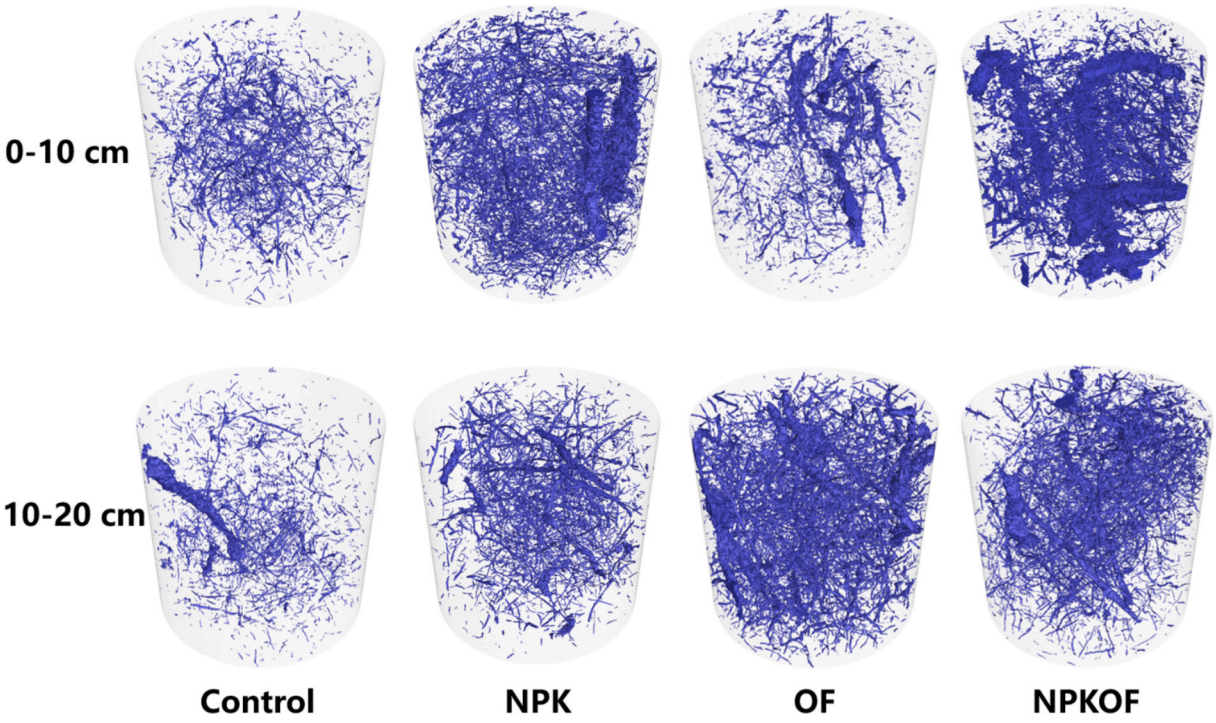

Fig. 3. 3D distributions of biopores (blue part) under different fertilization regimes. NPK, OF and NPKOF indicate treatments of chemical fertilizations, organic fertilization, and combined chemical fertilization with organic fertilization, respectively.

increasing POM-macropore distance, whereas root-derived POM displayed a linear positive relationship with root-derived POM-macropore distance ($P < 0.01$, Fig. 10).

4. Discussions

4.1. Effects of fertilization on macropores and biopores

Our study demonstrated that chemical or organic fertilization under conservation tillage significantly altered the macropore structure in the 0–10 cm soil layer, resulting in greater porosity and enhanced macropore connectivity (Fig. 2, Table 2). These improvements primarily resulted from structural modifications induced by crop root growth and residue decomposition. Notably, the NPK and NPKOF treatments achieved the highest crop yields (Fig. 8), consequently returning substantial crop residues to the soil after harvest. The decomposition of these organic materials significantly promoted new macropore formation while facilitating the development of a loose, porous structure through the combination of organic material and soil particles (Ding et al., 2025a; Phalempin et al., 2022; Witzgall et al., 2021). Furthermore, the accumulation of substantial fresh POM and roots can stimulate the activity of macrofauna (Le Mer et al., 2022), such as earthworms and orthoptera (Fig. S3), whose activities promote the formation of macropores. Contrastingly, numerous studies have reported minimal effects of inorganic fertilizers on macropore structure improvement (Yu et al., 2025; Fang et al., 2024). This discrepancy likely stems from straw removal in those studies, where the absence of organic inputs combined with the dispersive effects of fertilizer-derived ions exacerbated soil compaction and structural degradation (Guo et al., 2022). Although OF treatment yielded less than NPK and NPKOF, its substantial organic inputs still significantly enhanced soil structure. These findings align with previous research demonstrating the positive effects of organic and combined organic–inorganic fertilizers on soil structure (Zhou et al., 2016; Leuther et al., 2022). In the study, NPK and NPKOF treatments significantly enhanced biopore characteristics in the 0–10 cm soil layer, including bioporosity and length density (Fig. 4; Table 3). These findings correlate well with our crop yield data (Fig. 8), as both treatments markedly promoted crop growth and root system development. We deduced that organic management further enriched the biopore network by stimulating soil fauna activity (e.g., earthworms, nematodes) (Schlüter et al., 2022a; Pelosi et al., 2017). Certain soil fauna-generated pores exhibit non-cylindrical morphologies (Mele et al., 2021), which could not be quantified in our study due to limitations in the current image analysis methodology. Future studies could employ deep learning segmentation models (e.g., U-Net; Phalempin et al., 2025b) to identify these excluded pore types.

In the 10–20 cm layer, bioporosity and biopore length density were significantly greater under the OF and NPKOF treatments relative to the control (Fig. 4, Table 3). This result demonstrates the role of organic fertilization in promoting the development of subsoil pore structure. A striking observation was the higher proportion of biopores in the subsoil than in the topsoil under OF treatment (Fig. 4). This vertical distribution can be attributed to distinct pore-forming processes: in the topsoil, the pore network was dominated (92.04 %) by non-biopores derived from the decomposition of surface organic matter, whereas in the subsoil, biopores constituted a substantially larger proportion (41.3–44.6 %) of the porosity. This phenomenon primarily stems from fertilization promoting root penetration into the subsoil and enhancing soil fauna activity, thereby facilitating biopore formation. Within the dense Vertisol subsoil (Table 1), these biopores are indispensable for water and gas exchange (Zhang et al., 2019). As the dominant component of percolating pores in the 10–20 cm layer (Fig. S4), their development under organic fertilization ensures efficient solute transport, which is ultimately governed by the critical macropore diameter (Koestel, 2018a). As the experimental site has been under long-term no-till management, existing biopores persist over time. Consequently, these subsoil biopores may represent a cumulative result of repeated root growth and decomposition cycles over the past eight years.

4.2. Effects of fertilization on POM distributions

Our study confirmed that chemical fertilization and organic

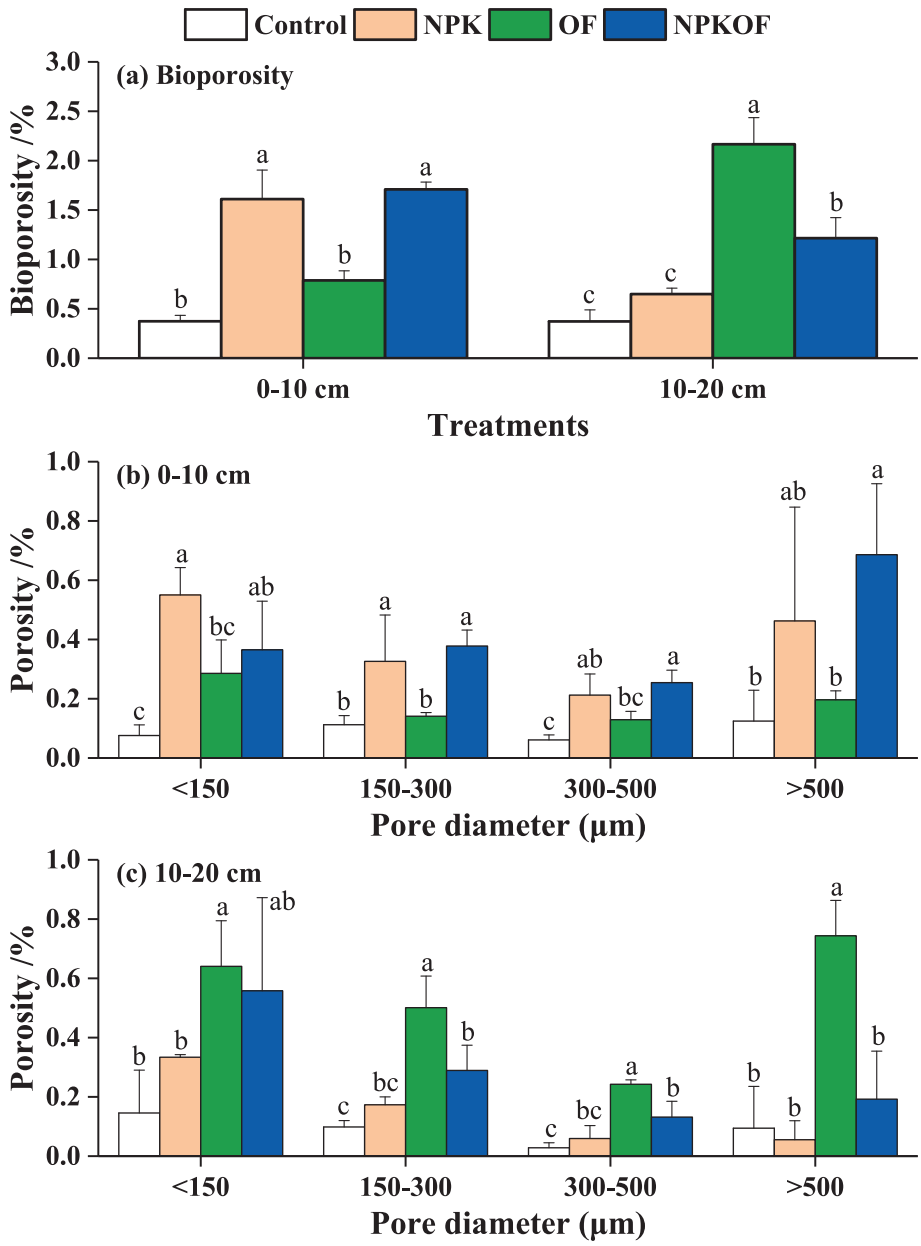

Fig. 4. Bioporosity and biopore size distributions under different fertilization regimes. NPK, OF and NPKOF indicate treatments of chemical fertilizations, organic fertilization, and combined chemical fertilization with organic fertilization, respectively. Different lowercase letters indicate significant differences among various fertilization regimes ($P < 0.05$).

Table 3
Biopore characteristic parameters under different fertilization regimes. NPK, OF and NPKOF indicate treatments of chemical fertilizations, organic fertilization, and combined chemical fertilization with organic fertilization, respectively. Different lowercase letters indicate significant differences among various fertilization regimes ($P < 0.05$).

Biopore	Treatments	Proportions of biopores/ %	Mean biopore diameter /μm	Hydraulic radius /μm	Surface area density /mm^{-1}	Length density /mm^{-2}
0–10 cm	Control	10.9 (4.45) a	459 (231) a	74.4 (26.0) a	0.05 (0.01) c	0.06 (0.01) b
	NPK	13.4 (4.31) a	853 (380) a	92.2 (9.44) a	0.06 (0.02) c	0.19 (0.03) a
	OF	7.96 (4.20) a	646 (136) a	88.8 (15.0) a	0.17 (0.03) a	0.10 (0.01) b
	NPKOF	14.3 (1.41) a	891 (37.2) a	109 (4.32) a	0.10 (0.00) b	0.17 (0.05) a
10–20 cm	Control	22.5 (7.33) b	260 (14.0) b	67.9 (19.6) b	0.09 (0.03) b	0.02 (0.00) c
	NPK	42.2 (9.16) a	404 (131) b	65.8 (3.64) b	0.20 (0.04) a	0.05 (0.01) c
	OF	44.6 (7.88) a	892 (79.5) a	109 (18.7) a	0.16 (0.01) ab	0.18 (0.02) a
	NPKOF	41.3 (6.47) a	683 (190) a	83.1 (26.1) ab	0.16 (0.07) ab	0.13 (0.01) b

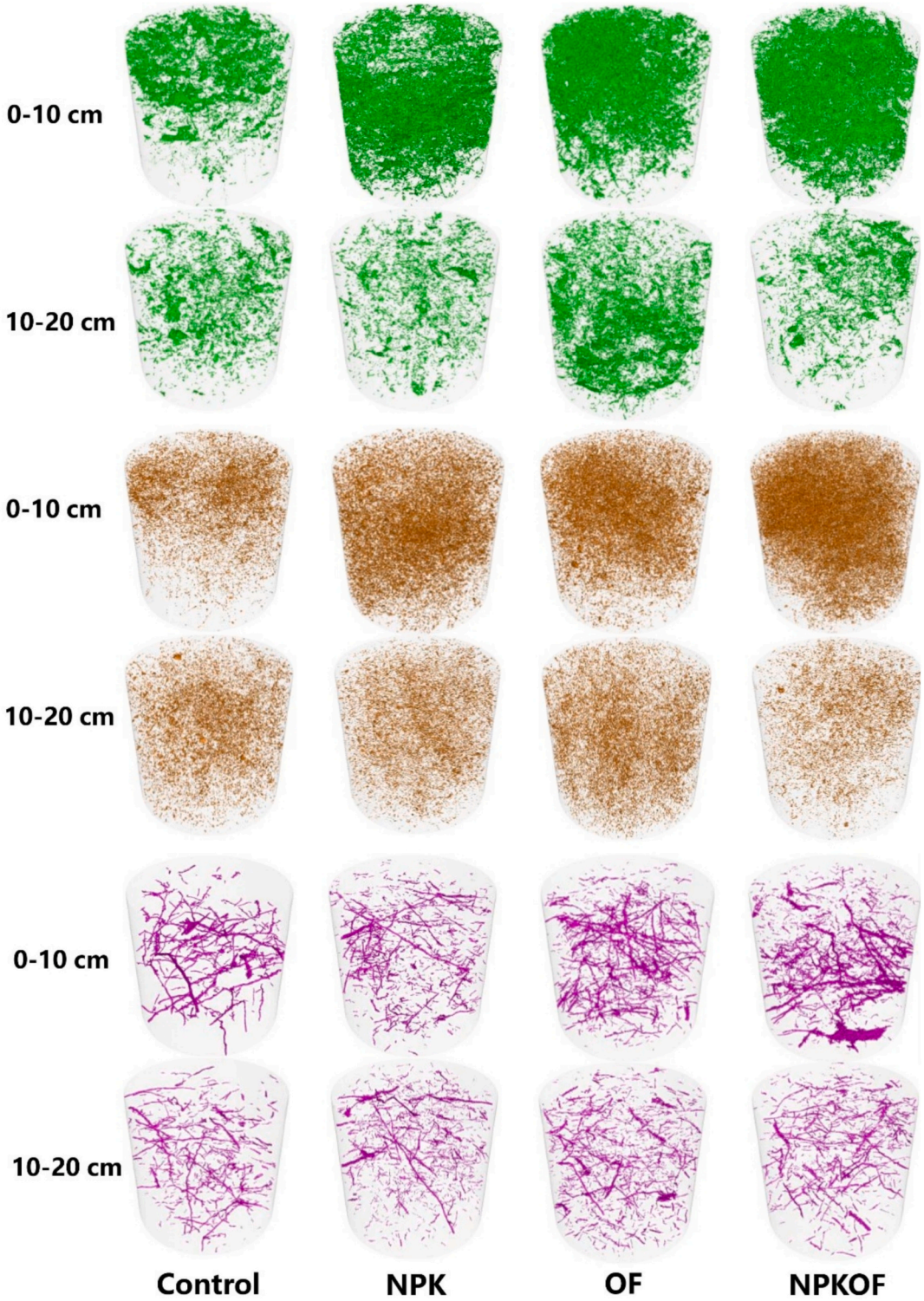

Fig. 5. 3D distributions of fresh POM (green part), decomposed POM (brown part) and root-derived POM (pink part) under different fertilization regimes. NPK, OF and NPKOF indicate treatments of chemical fertilizations, organic fertilization, and combined chemical fertilization with organic fertilization, respectively.

fertilization significantly increased the accumulation of fresh POM in the 0–10 cm layer (Fig. 6). This is primarily attributed to the fact that both chemical fertilizers and organic amendments enhance crop and root growth, thereby substantially increasing above- and belowground biomass returned to the soil (Tang et al., 2023). These organic inputs serve as a key source of fresh POM, significantly promoting its accumulation as evidenced by straw-derived C input (Fig. 8). Furthermore, in the OF and NPKOF treatments, the organic amendments themselves contained abundant coarse organic materials, which directly contributed to fresh POM incorporation into the soil. This finding aligns with previous studies (Celik et al., 2010; Leuther et al., 2022; Schlüter et al., 2022a), which suggest that increased organic carbon is often associated with the transition to organic farming, primarily due to organic manure inputs. Evidence indicates these organic materials enhance soil aggregation (Guo et al., 2019; Sodhi et al., 2009), reducing disturbances to aggregates caused by frequent wet-dry cycles and improving the

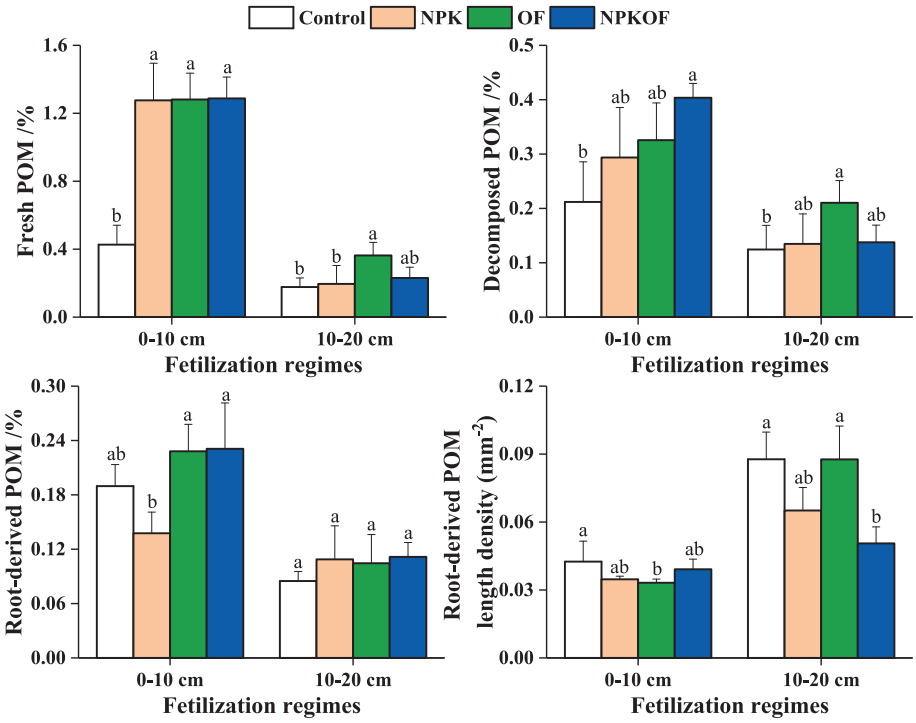

Fig. 6. Content of fresh POM, decomposed POM, root-derived POM and root-derived POM length density under different fertilization regimes. NPK, OF and NPKOF indicate treatments of chemical fertilizations, organic fertilization, and combined chemical fertilization with organic fertilization, respectively. Different lowercase letters indicate significant differences among various fertilization regimes ($P < 0.05$).

protection of POM and SOC. Additionally, NPKOF treatment significantly increased decomposed POM in the 0–10 cm soil layer (Fig. 6), primarily derived from the further breakdown of organic fertilizer particles and fresh residues. While previous studies have identified biochar as a potential major component of decomposed POM (Schlüter et al., 2022b), this scenario was excluded in our study site due to the absence of fire events. Consequently, organic fertilizer inputs emerged as the predominant factor enhancing both fresh and decomposed POM fractions in surface soils. Additionally, it was observed that the control treatment did not significantly reduce the root-derived POM content in the 0–10 cm soil layer compared to other treatments. Under the no-fertilization condition, crops may develop more extensive root systems to seek additional nutrients.

The concentration of root-derived POM in the 0–10 cm layer was significantly higher in the OF and NPKOF treatments compared to the NPK treatment ($P < 0.05$). This pattern likely results from organic amendments reducing soil bulk density, thereby decreasing mechanical impedance to root proliferation. Furthermore, compared to the control, OF significantly enhanced root residue decomposition and fragmentation in the 0–10 cm soil layer. This observation was proved by 3D root distribution, which revealed abundant fragmented root segments (Fig. 5). The accelerated decomposition probably resulted from improved microbial activity stimulated by micro-nutrients present in organic fertilizers. However, no significant differences in root-derived POM content were observed in the 10–20 cm layer (Fig. 6). Vertisols are characterized by high swelling-shrinkage capacity and strength (Wang et al., 2022), and exhibit strong vertical stratification of SOC and POM under long-term no-till management. Schlüter et al. (2018) reported that long-term no-tillage did not improve deep soil structure but instead led to the formation of a more compact and less permeable no-till pan beneath the plow layer. These physical constraints result in preferential accumulation of root-derived C input in surface soils, while significantly constraining root-derived POM accumulation in subsoil layers. Consequently, despite substantial surface organic inputs, limited downward translocation of organic materials occurred, resulting in constrained POM accumulation in the subsurface layer.

4.3. Links between POM and macropores, biopores

Positive correlations between three POM fractions and macropore structure characteristics (image-based porosity, connected porosity, hydraulic radius, and connection probability) were observed in the study (Fig. 9; Fig. S2). This indicated POM accumulation had positive effects on macropore development. POM contains abundant cementing substances that bind with soil particles to create a well-structured pore network. Upon decomposition, these organic materials generated additional pores, enhancing macropore connectivity (Ding et al., 2025a). The developed macropore networks may subsequently facilitate water and gas exchange, creating optimal habitats for microbial and faunal activity (Lee et al., 2024b). Our study also revealed a significant positive correlation between macropore structure and air conductivity, and the critical macropore diameter was found to govern water movement (Fig. 9; Fig. S5). This improved macropore architecture further establishes favorable physical conditions for POM decomposition. Fresh POM primarily consists of root residues and straw fragments. The shorter fresh POM-macropore distance indicated closer proximity to macropore spaces (Fig. S1), granting preferential access to water and oxygen that accelerates microbial decomposition of fresh POM (Rohe et al., 2021). In contrast, decomposed POM consisted of more fragmented materials located farther from pore surfaces. Both fresh and decomposed POM fractions exhibited significant negative correlations with macropore distance (Fig. 10), demonstrating they tend to accumulate around macropores, with their decomposition being regulated by pore structure characteristics. While organic fertilizer application introduced substantial organic inputs, it simultaneously reduced the physical distance between POM and soil pores (Fig. 7). This process simultaneously facilitates significant POM depletion through the creation of optimal physical conditions for decomposition. Thus, long-term organic fertilizer input is essential for the accumulation of both fresh and decomposed POM fractions. Root-derived POM was positively correlated with

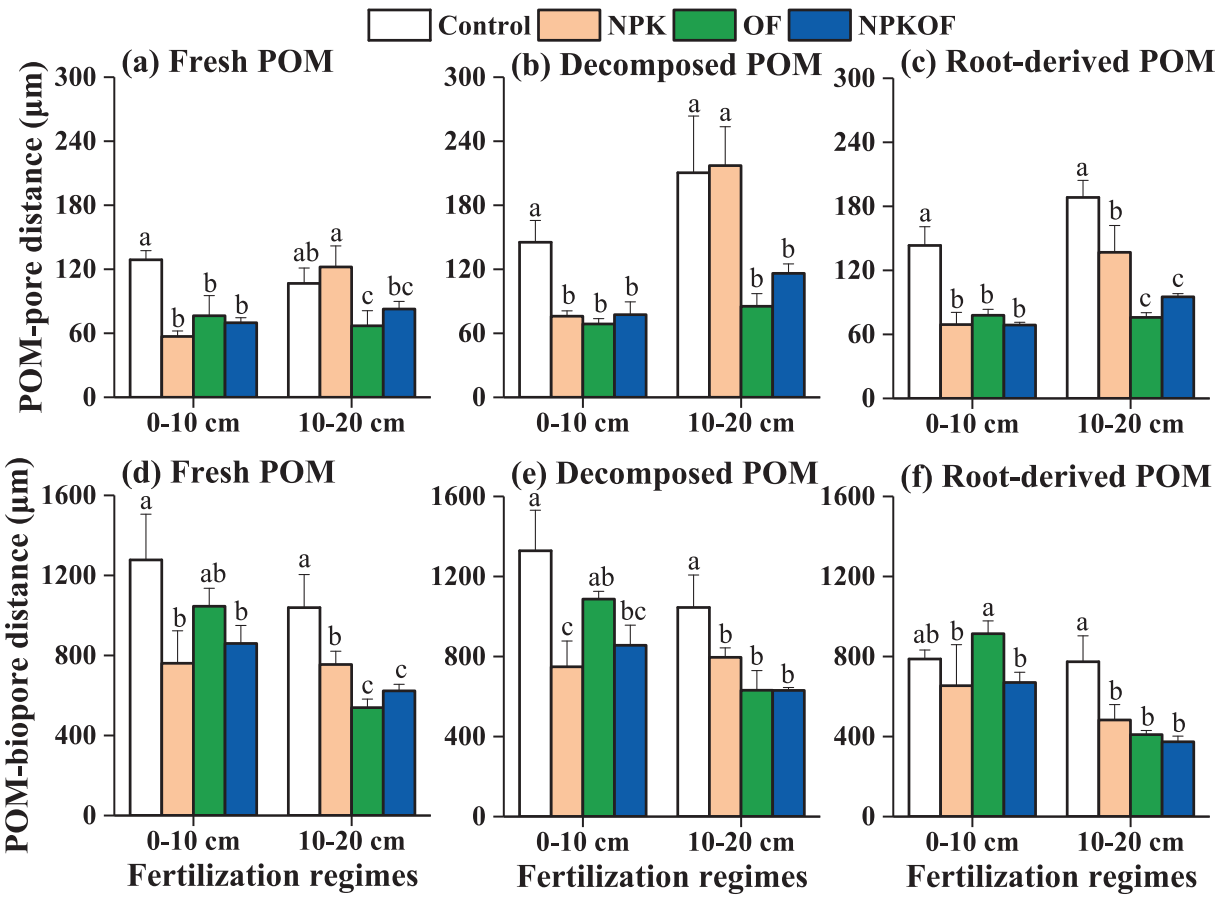

Fig. 7. POM-macropore distance (a-c) and POM-biopore distance (d-f) under different fertilization regimes. NPK, OF and NPKOF indicate treatments of chemical fertilizations, organic fertilization, and combined chemical fertilization with organic fertilization, respectively. Different lowercase letters indicate significant differences among various fertilization regimes ($P < 0.05$).

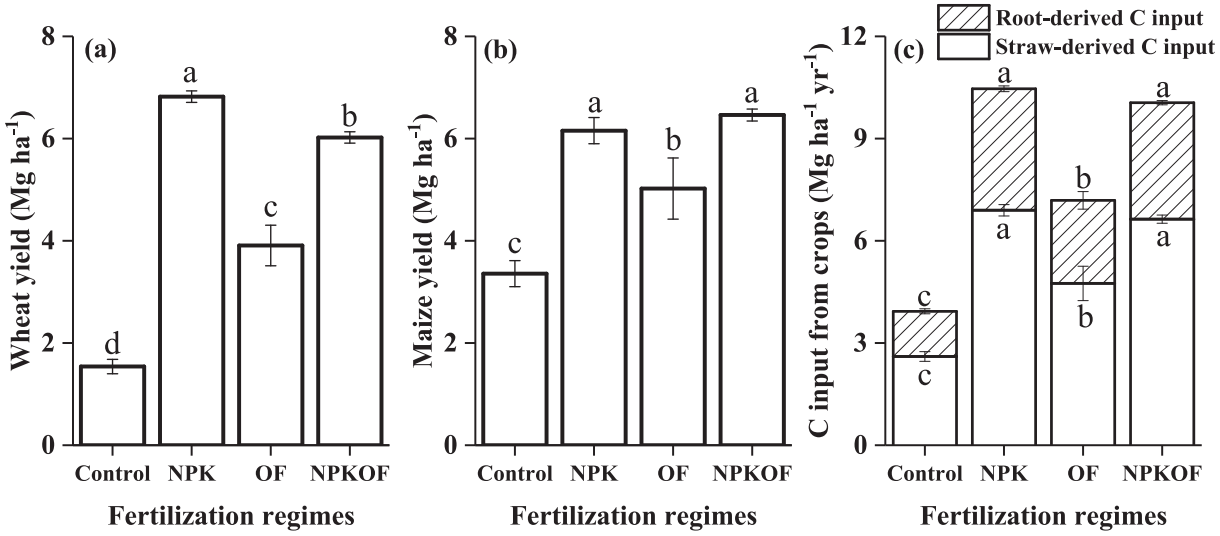

Fig. 8. Wheat and maize yields (2022–2024 average values) and carbon (C) input from crops. NPK, OF and NPKOF indicate treatments of chemical fertilizations, organic fertilization, and combined chemical fertilization with organic fertilization, respectively. Different lowercase letters indicate significant differences among various fertilization regimes ($P < 0.05$).

macropore structure, indicating that well-developed macropore networks for root-derived POM not only enhanced decomposition but also maintained continuous replenishment through promoted root proliferation.

Contrary to our hypothesis, the study revealed no significant positive correlations between root-derived POM and biopore parameters (Fig. 9, Fig. S2, Table S13). Although biopores are primarily formed by root growth and decay or by soil macrofauna activity, we observed only weak

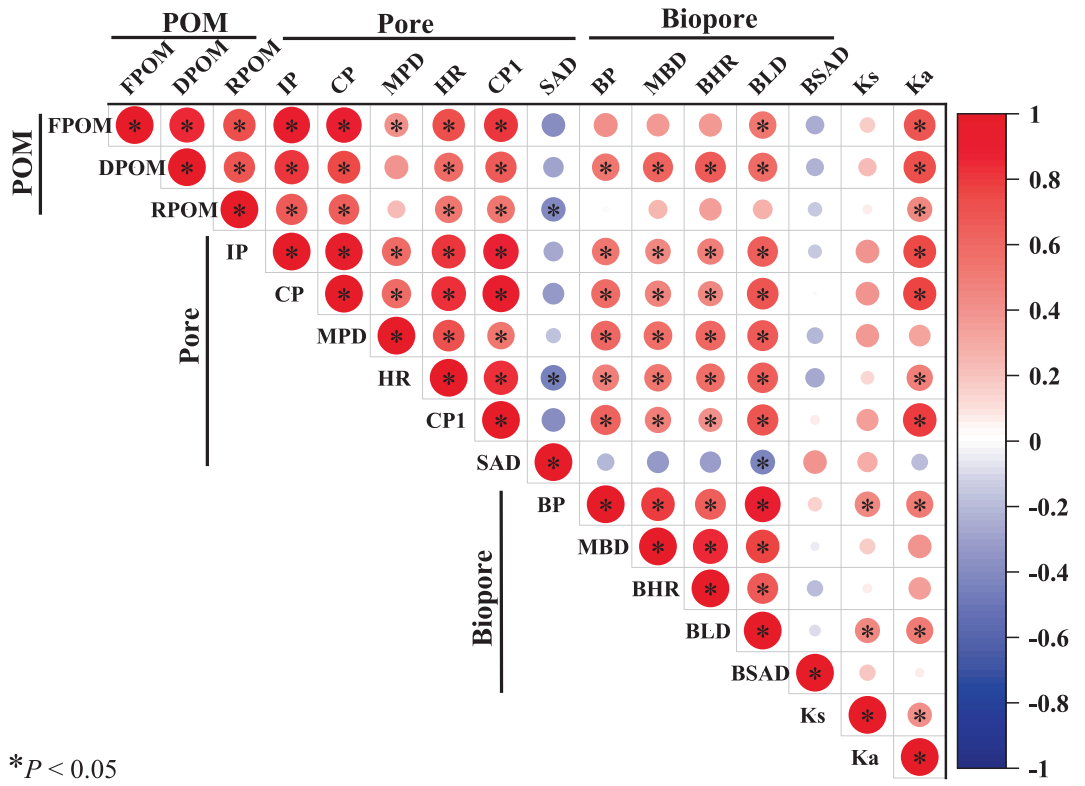

Fig. 9. Spearman correlations among POM, macropore structures, biopore characteristics. FPOM: fresh POM. DPOM: decomposed POM; RPOM: root-derived POM; IP: image-based porosity; MPD: mean pore diameter; HR: hydraulic radius; CP: connected porosity; CP1: connection probability; SAD: surface area density; BP: bioporosity; MBD: mean biopore diameter; BHR: biopore hydraulic radius; BLD: biopore length density; K_s: saturated hydraulic conductivity; K_a: air permeability.

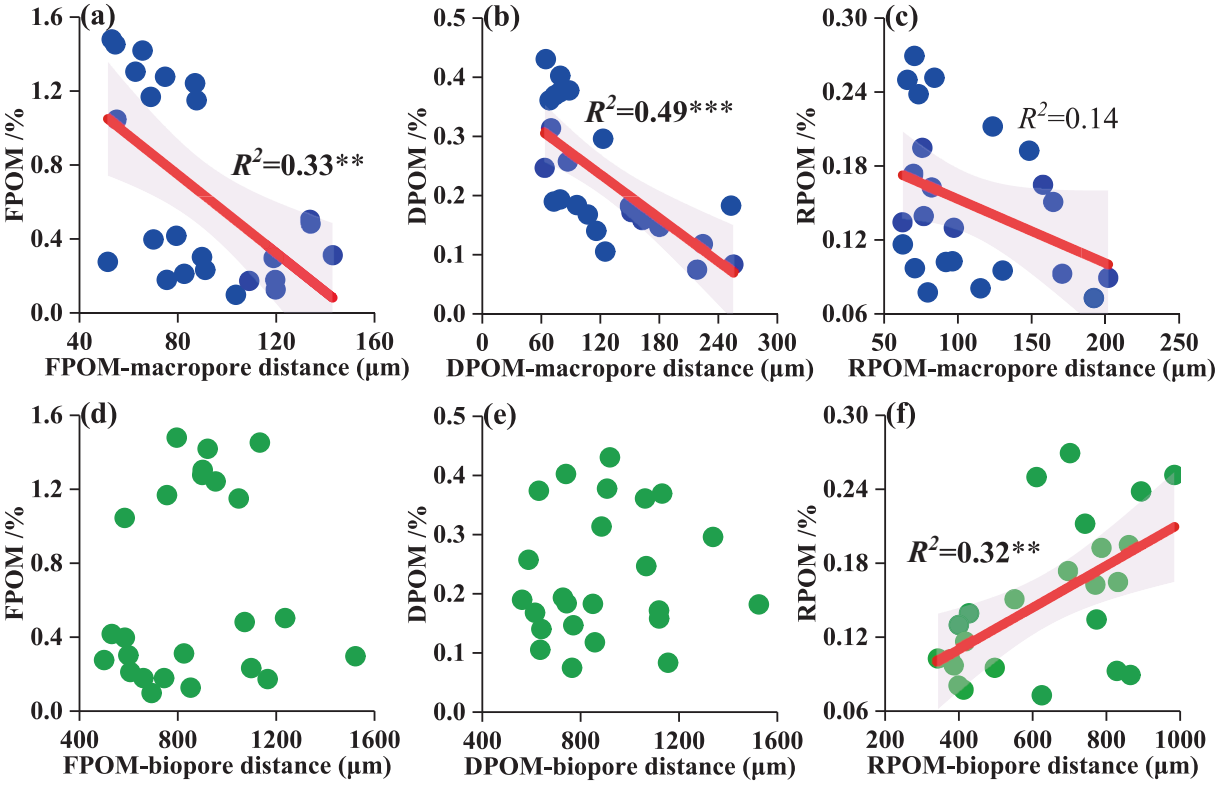

Fig. 10. Linear correlations between POM and POM-pore distance (a-c), POM-biopore distance (d-f). **, and *** indicate significant correlations at $P < 0.01$, and $P < 0.001$ level. FPOM: fresh POM; DPOM: decomposed POM; RPOM: root-derived POM.

associations between these features. This was because long-term no-till management led to substantial biopore accumulation in the subsoil layer (41.3 %-44.6 % proportions across fertilization treatments, Table 3), yet this did not translate to significant increases in root density, likely constrained by high bulk density (1.62–1.65 g cm^{-3}) of these soil layers, which is commonly associated with large penetration resistance. Root-derived POM increased with distance from biopores (Fig. 10), indicating greater root accumulation in areas farther from biopores. Biopores are known to provide preferential pathways for root growth and development, while the nutrient-rich biopore sheath can promote microbial-mediated root decomposition (Petzoldt et al., 2022; Xiong et al., 2022). However, biopores exhibited limited hydraulic conductivity and gas permeability that may have led to reduced microbial activity in the subsoil (Table 1). Consequently, roots located farther from biopores may have been preserved in the soil due to reduced microbial decomposition. As critical components of the macropore network, increased biopore volume significantly improved overall macropore connectivity. This enhancement particularly accelerated the decomposition of fresh and decomposed POM in surface soil. However, while biopores constituted the dominant structure of the subsoil macropore network under organic fertilization, they exerted no significant influence on root-derived POM dynamics.

4.4. Limitations and prospects

This study quantitatively analyzed the characteristics of biopores and their relationship with POM. Based on morphological features, we successfully segmented biopores that typically exhibit continuous, straight cylindrical shapes. Biopores are known to be formed through soil faunal burrowing activity and root channeling. Numerous studies have established that biopores serve as preferential pathways for root growth, thereby facilitating root-derived POM accumulation (Colombi et al., 2017; Xiong et al., 2022; Atkinson et al., 2019). However, our findings revealed significant POM accumulation in areas distal to biopores. This apparent contradiction highlights the need for mechanistic analysis of how biopores regulate microbial-mediated root decomposition dynamics. Additionally, in cases where roots completely occupied existing biopores, imaging analysis identified these structures as root material, which was located far from other biopores. Furthermore, when roots are not consumed or decomposed by soil fauna or microorganisms, they are often located at a greater distance from biopores. Due to inherent limitations in the experimental design, this phenomenon was not quantitatively characterized. Future research should investigate the role of biopores in POM decomposition and accumulation processes, which may hold important implications for nutrient cycling and yield enhancement in conservation agriculture systems.

5. Conclusions

In summary, our study quantified the effects of long-term organic fertilization under conservation tillage on soil macropore and biopore structure and classified POM (fresh POM, decomposed POM, and root-derived POM) distributions and their relationships using X-ray CT scanning. Our findings revealed that organic fertilization treatments (OF, NPKOF) were associated with the accumulation of fresh and root-derived POM, as well as a greater abundance of macropore and biopore structures in the 0–10 cm layer. The OF treatment was also linked to improved macropore and biopore structures in the 10–20 cm layer. However, organic fertilization (OF and NPKOF) reduced POM-pore distances, indicating increased susceptibility to decomposition, which contributed to the development of macropore structure. Although organic fertilization decreased the distance between root-derived POM and biopores, no significant correlation was observed between root-derived POM and biopore characteristics. Root-derived POM primarily accumulated in areas distant from biopores. Our findings highlight that organic fertilization is an important factor linked to improved soil pore structure and POM accumulation in Vertisols. While POM accumulation creates favorable conditions for macropore development, our results showed no significant effect of biopores on root-derived POM distribution. The dynamics of root-derived POM influenced by macropores and biopores required further investigations to provide insights for organic carbon accumulation in conservation agriculture systems.

CRediT authorship contribution statement

Tianyu Ding: Writing – review & editing, Writing – original draft, Visualization, Software, Resources, Methodology, Data curation, Conceptualization. **Zichun Guo:** Writing – review & editing, Visualization, Validation, Project administration, Investigation, Funding acquisition, Data curation, Conceptualization. **John Koestel:** Writing – review & editing, Validation, Software, Methodology. **Jiaqi Li:** Visualization, Resources, Data curation. **Jianli Liu:** Visualization, Validation, Supervision. **Xinhua Peng:** Writing – review & editing, Validation, Supervision, Project administration, Funding acquisition.

Declaration of competing interest

The authors declare that they have no known competing financial interests or personal relationships that could have appeared to influence the work reported in this paper.

Acknowledgements

We gratefully acknowledge the anonymous reviewers for reviewing the manuscript that has been greatly improved thereafter. This study was granted by National Key Research and Development Program (2023YFD1900204, 2023YFD1900201), and the Self-deployed Project of Institute of Soil Science, Chinese Academy of Sciences (ISSASIP2214).

Appendix A. Supplementary data

Supplementary data to this article can be found online at https://doi.org/10.1016/j.geoderma.2025.117602.

Data availability

Data will be made available on request.

References

Atkinson, J.A., Hawkesford, M.J., Whalley, W.R., Zhou, H., Mooney, S.J., 2019. Soil strength influences wheat root interactions with soil macropores. Plant Cell Environ. 43, 235–245.

Behringer, M., Koestel, J., Muys, B., Wriessnig, K., Bieringer, M., Schlogl, M., Katzensteiner, K., 2025. A long road to soil health restoration: earthworms and soil structure show partial recovery in 18-year-old forest skid trails. Soil Biol. Biochem. 210, 109953.

Berg, S., Kutra, D., Kroeger, T., Straehle, C.N., Kausler, B.X., Haubold, C., Schiegg, M., Ales, J., Beier, T., Rudy, M., Eren, K., Cervantes, J.I., Xu, B., Beuttenmueller, F., Wolny, A., Zhang, C., Koethe, U., Hamprecht, F.A., Kreshuk, A., 2019. Ilastik: interactive machine learning for (bio)image analysis. Nat. Methods 16, 1226–1232.

Capowiez, Y., Gilbert, F., Vallat, A., Poggiale, J.C., Bonzom, J.M., 2021. Depth distribution of soil organic matter and burrowing activity of earthworms–mesocosm study using X-ray tomography and luminophores. Biol. Fertil. Soils 57 (3), 337–346.

Celik, I., Gunal, H., Budak, M., Akpinar, C., 2010. Effects of long-term organic and mineral fertilizers on bulk density and penetration resistance in semi-arid Mediterranean soil conditions. Geoderma 160, 236–243.

Ding, T.Y., Guo, Z.C., Qian, Y.Q., Wang, Y.K., Jiang, F.H., Zhang, Z.B., Peng, X.H., 2025a. Interaction between POM and pore structure during straw decomposition in two soils with contrasting texture. Soil Tillage Res. 245, 106288.

Ding, T.Y., Guo, Z.C., Li, W., Peng, X.H., 2025b. Long-term straw return with nitrogen fertilization enhances soil pore structure, POM accumulation, and their positive feedback in a Vertisol. Soil Tillage Res. 252, 106602.

Fang, H., Zhang, N., Yu, Z., Li, D., Peng, X., Zhou, H., 2024. Micro-CT Analysis of Pore Structure in Upland Red Soil under Different Long-Term Fertilization Regimes. Agronomy 14, 2668.

Colombi, T., Braun, S., Keller, T., Walter, A., 2017. Artificial macropores attract crop roots and enhance plant productivity on compacted soils. Sci. Total Environ. 574, 1283–1293.
Guo, Z.C., Li, W., Islam, M.U., Wang, Y.K., Zhang, Z., Peng, X.H., 2022. Nitrogen fertilization degrades soil aggregation by increasing ammonium ions and decreasing biological binding agents on a Vertisol after 12 years. Pedosphere 32 (4), 629–636.
Guo, Z.C., Zhang, J.B., Fan, J., Yang, X.Y., Yi, Y.L., Han, X.R., Wang, D.Z., Zhu, P., Peng, X.H., 2019. Does animal manure application improve soil aggregation? Insights from nine long-term fertilization experiments. Sci. Total Environ. 660, 1029–1037.
Hua, K., Wang, D., Guo, X., Guo, Z., 2014. Carbon sequestration efficiency of organic amendments in a long–term experiment on a vertisol in Huang–Huai–Hai Plain. China. Plos One 9 (9), e108594.
IPCC guidelines for national greenhouse gas inventories. 2006. Prepared by the national greenhouse gas inventories programme. In: Eggleston HS, Buendia L, Miwa K, Ngara T and Tanabe K (Eds), Institute for Global Environmental Strategies. IPCC, Hayama, Japan.
Jiang, F., Xue, X., Zhang, L., Zuo, Y., Zhang, H., Zheng, W., Bian, L., Hu, L., Hao, C., Du, J., Ci, Y., Cheng, R., Dawa, C., Biswas, M., Islam, M.U., Meng, F., Peng, X., 2024. Soil wind erosion, nutrients, and crop yield response to conservation tillage in North China: a field study in a semi-arid and wind erosion region after 9 years. Field Crops Res. 316, 109508.
Kautz, T., 2014. Research on subsoil biopores and their functions in organically managed soils: a review. Renewable Agric. Food Syst 30, 318–327.
Koestel, J., 2018a. SoilJ: an ImageJ plugin for the semiautomatic processing of three-dimensional X-ray images of soils. Vadose Zone J. 17 (1), 1–7.
Koestel, J., Dathe, A., Skaggs, T.H., Klakegg, O., Ahmad, M.A., Babko, M., Gimenez, D., Farkas, C., Nemes, A., Jarvis, N., 2018b. Estimating the permeability of naturally structured soil from percolation theory and pore space characteristics imaged by X-ray. Water Resour. Res. 54 (11), 9255–9263.
Kravchenko, A.N., Guber, A.K., 2017. Soil pores and their contributions to soil carbon processes. Geoderma 287, 31–39.
Kravchenko, A.N., Negassa, W.C., Guber, A.K., Rivers, M.L., 2015. Protection of soil carbon within macro-aggregates depends on intra-aggregate pore characteristics. Sci. Rep. 5, 16261.
Larsbo, M., Koestel, J., Jarvis, N., 2014. Relations between macropore network characteristics and the degree of preferential solute transport. Hydrol. Earth Syst. Sci. 18 (12), 5255–5269.
Lavallee, J.M., Soong, J.L., Cotrufo, M.F., 2020. Conceptualizing soil organic matter into particulate and mineral-associated forms to address global change in the 21st century. Glob. Chang. Biol. 26, 261–273.
Lee, J.H., Geers-Lucas, M., Guber, A.K., Kravchenko, A.N., 2024a. Pore structures in detritusphere of soils under switchgrass and restored prairie vegetation community. Land Degrad. Dev. 35, 5817–5829.
Lee, J.H., Ulbrich, T.C., Geers-Lucas, M., Robertson, G.P., Guber, A.K., Kravchenko, A.N., 2024b. Very fine roots differ among switchgrass (*Panicum virgatum L.*) cultivars and differentially affect soil pores and carbon processes. Soil Biol. Biochem. 199, 109610.
Legland, D., Arganda-Carreras, I., Andrey, P., 2016. MorphoLibJ: integrated library and plugins for mathematical morphology with ImageJ. Bioinformatics 32, 3532–3534.
Le Mer, G., Bottinelli, N., Dignac, M., Capowiez, Y., Jouquet, P., Mazurier, A., Baudin, F., Caner, L., Rumpel, C., 2022. Exploring the control of earthworm cast macro- and micro-scale features on soil organic carbon mineralization across species and ecological categories. Geoderma 427, 116151.
Leuther, F., Wolff, M., Kaiser, K., Schumann, L., Merbach, I., Mikutta, R., Schlüter, S., 2022. Response of subsoil organic matter contents and physical properties to long-term, high-rate farmyard manure application. Eur. J. Soil Sci. 73 (2), e13233.
Leuther, F., Mikutta, R., Wolff, M., Kaiser, K., Schlüter, S., 2023. Structure turnover times of grassland soils under different moisture regimes. Geoderma 433, 116464.
Liu, C., Si, B., Zhao, Y., Wu, Z., Lu, X., Chen, X., Han, X., Zhu, Y., Zou, W., 2025. Drivers of soil quality and maize yield under long-term tillage and straw incorporation in Mollisols. Soil Tillage Res. 246, 106360.
Lu, R.K., 2000. Analytical Methods of Soil Agrochemistry. China Agricultural Science and Technology Press, Beijing.
Lucas, M., Schlüter, S., Vogel, H.J., Vetterlein, D., 2019. Soil structure formation along an agricultural chronosequence. Geoderma 350, 61–72.
Lucas, M., Santiago, J.P., Chen, J., Guber, A., Kravchenko, A., 2023. The soil pore structure encountered by roots affects plant-derived carbon inputs and fate. New Phytol. 240 (2), 515–528.
Mele, G., Buscemi, G., Gargiulo, L., Terribile, F., 2021. Soil burrow characterization by 3D image analysis: Prediction of macroinvertebrate groups from biopore size distribution parameters. Geoderma 404, 115292.
NCATS, 1999. Chinese organic fertilizer handbook. National Center for Agricultural Technology Service, Chinese Agricultural Publisher. (In Chinese).
Pelosi, C., Grandeau, G., Capowiez, Y., 2017. Temporal dynamics of earthworm-related macroporosity in tilled and non-tilled cropping systems. Geoderma 289, 169–177.
Peng, X.H., Zhang, Z.Z., Guo, Z.C., 2022. The mechanism and technology for improving Shajiang black soil. Science Press, Beijing.
Petzoldt, L., Kroschewski, B., Kautz, T., 2022. Metabolic activity of Hordeum vulgare, Brassica napus and Vicia faba in Worm and root type Biopore Sheaths. Plant and Soil 472, 565–575.
Phalempin, M., Jentzsch, N., Kohne, J.M., Schreiter, S., Gründling, R., Vetterlein, D., Schlüter, S., 2025a. Soil structure development in a five-year chronosequence of maize cropping on two contrasting soil textures. Soil Tillage Res. 251, 106561.
Phalempin, M., Krämer, L., Gerrs-Lucas, M., Isensee, F., Schlüter, S., 2025b. Deep learning segmentation of soil constituents in 3D X-ray CT images. Geoderma 458, 117321.
Phalempin, M., Landl, M., Wu, G.-M., Schnepf, A., Vetterlein, D., Schlüter, S., 2022. Maize root-induced biopores do not influence root growth of subsequently grown maize plants in well aerated, fertilized and repacked soil columns. Soil Tillage Res. 221, 105398.
Rabot, E., Wiesmeier, M., Schlüter, S., Vogel, H.J., 2018. Soil structure as an indicator of soil functions: a review. Geoderma 314, 122–137.
Renard, P., Allard, D., 2013. Connectivity metrics for subsurface flow and transport. Adv. Water Resour. 51, 168–196.
Ren, Z., Han, X., Feng, H., Wang, L., Ma, G., Li, J., Wang, C., 2024. Long-term conservation tillage improves soil stoichiometry balance and crop productivity based on a 17-year experiment in a semi-arid area of northern China. Sci. Total Environ. 908, 168283.
Rohe, L., Apelt, B., Vogel, H.-J., Well, R., Wu, G.-M., Schlüter, S., 2021. Denitrification in soil as a function of oxygen availability at the microscale. Biogeosciences 18 (3), 1185–1201.
Schlüter, S., Gil, E., Doniger, T., Applebaum, I., Steinberger, Y., 2022a. Abundance and community composition of free-living nematodes as a function of soil structure under different vineyard managements. Appl. Soil Ecol. 170, 104291.
Schlüter, S., Großmann, C., Diel, J., Wu, G.-M., Tischer, S., Deubel, A., Rücknagel, J., 2018. Long-term effects of conventional and reduced tillage on soil structure, soil ecological and soil hydraulic properties. Geoderma 332, 10–19.
Schlüter, S., Leuther, F., Albrecht, L., Hoeschen, C., Kilian, R., Surey, R., Mikutta, R., Kaiser, K., Mueller, C.W., Vogel, H.J., 2022b. Microscale carbon distribution around pores and particulate organic matter varies with soil moisture regime. Nat. Commun. 13, 2098.
Schlüter, S., Vogel, H.-J., 2016. Analysis of soil structure turnover with garnet particles and X-ray microtomography. PLoS One 11, e0159948.
Schindelin, J., Arganda-Carreras, I., Frise, E., Kaynig, V., Longair, M., Pietzsch, T., Preibisch, S., Rueden, C., Saalfeld, S., Schmid, B., Tinevez, J.Y., White, D.J., Hartenstein, V., Eliceiri, K., Tomancak, P., Cardona, A., 2012. Fiji: an open-source platform for biological-image analysis. Nat. Methods 9 (7), 676–682.
Sodhi, G.P.S., Beri, V., Benbi, D.K., 2009. Soil aggregation and distribution of carbon and nitrogen in different fractions under long-term application of compost in rice-wheat system. Soil Tillage Res. 103, 412–418.
Tang, B., Rocci, K.S., Lehmann, A., Rillig, M.C., 2023. Nitrogen increases soil organic carbon accrual and alters its functionality. Glob. Chang. Biol. 10, 744.
Wang, Y.K., Zhang, Z.B., Guo, Z.C., Xiong, P., Peng, X.H., 2022. The dynamic changes of soil air-filled porosity associated with soil shrinkage in a Vertisol. Eur. J. Soil Sci. e13313.
Witzgall, K., Vidal, A., Schubert, D.I., Hoschen, C., Schweizer, S.A., Buegger, F., Pouteau, V., Chenu, C., Mueller, C.W., 2021. Particulate organic matter as a functional soil component for persistent soil organic carbon. Nat. Commun. 12, 4115.
Xiong, P., Zhang, Z., Peng, X., 2022. Root and root-derived biopore interactions in soils: a review. J. Plant Nutr. Soil Sci. 185 (5), 643–655.
Yi, Y., 2009. Methods for Studying Soil Physics. Peking University Press, Beijing.
Yu, X.L., Zhang, X.M., Zhan, S.B., Lu, S.G., 2025. Configuration of pore structure and related functions in macroaggregates following long-term organic and inorganic fertilization. Soil Tillage Res. 247, 106368.
Zhang, Z.B., Liu, K.L., Zhou, H., Lin, H., Li, D.M., Peng, X.H., 2019. Linking saturated hydraulic conductivity and air permeability to the characteristics of biopores derived from X-ray computed tomography. J. Hydrol. 571, 1–10.
Zhang, Z., Peng, X., 2021. Bio-tillage: a new perspective for sustainable agriculture. Soil till. Res. 206, 104844.
Zhao, Y., Wang, M., Hu, S., Zhang, X., Ouyang, Z., Zhang, G., Huang, B., Zhao, S., Wu, J., Xie, D., Zhu, B., Yu, D., Pan, X., Xu, S., Shi, X., 2018. Economics- and policy-driven organic carbon input enhancement dominates soil organic carbon accumulation in Chinese croplands. PNAS 115 (16), 4045–4050.
Zhou, H., Fang, H., Mooney, S.J., Peng, X.H., 2016. Effects of long-term inorganic and organic fertilizations on the soil micro and macro structures of rice paddies. Geoderma 266, 66–74.